Range of Validity of the Entropic Spring Concept in Polymer Melt Relaxation

J. Gao and J. H. Weiner*

Division of Engineering and Department of Physics, Brown University, Providence, Rhode Island 02912

Received January 2, 1992; Revised Manuscript Received March 20, 1992

ABSTRACT: Computer simulations of stress relaxation in a model polymer melt demonstrate that the entropic spring concept and the Rouse model greatly underestimate the stress in the glassy and transition regimes and become accurate only in the rubbery and terminal regimes. The time-dependent segment orientation in a time-dependent elongational deformation of this model is also studied. The ratio of orientation to stress is smaller (by a factor of ~35) in the glassy regime than in the rubbery and terminal regimes.

1. Introduction

The concept of a long-chain molecule acting as an entropic spring has played a central role in polymer science since its introduction by Guth and Mark[1] almost 60 years ago. Briefly, the concept deals with the force f that must be imposed on the end atoms of an isolated long-chain molecule to maintain them at a fixed end-to-end distance r. Under the assumption that the internal energy of the chain is independent of r, we are led by thermodynamics to the relation

$$f = -T\frac{\partial S}{\partial r} \tag{1}$$

where $S(r)$ is the configurational entropy of the chain at end-to-end distance r. It is natural, then, to regard the macromolecule as acting as an entropic spring (that is, the spring force is due to a change in entropy rather than energy) with the tensile force in the spring transmitted through the covalent backbone of the chain.

Most theoretical treatments of viscoelasticity in dense polymeric systems ascribe the stress to the force acting in the covalent bonds of the long-chain molecules, based on the concept that these molecules act as entropic springs. Excluded-volume (EV) interactions are assumed to contribute only a hydrostatic pressure to the system and are generally neglected.

We have been reexamining this assumption through the computer simulation of model polymeric systems, beginning first with the equilibrium regime of rubber elasticity. These simulations[2,3] revealed the surprising result that, at realistic system densities, the deviatoric stress, i.e., the total stress minus the mean stress, is due primarily to the screened EV interactions and not to the covalent interactions. We also found, however, that, although the physical picture was thus very different from the usual one, the equilibrium stress in rubberlike solids as computed on the basis of the classical entropic spring concept was numerically quite close, at small extension, to that found in the simulations and generated by the EV interactions. At large extensions these interactions do cause small deviations from the simple entropic spring predictions; these may be responsible, at least in part, for the experimentally observed deviations from the classical theory of rubber elasticity.[3]

Most recently[4] we have extended these simulations to the viscoelastic, nonequilibrium regime. There, too, we find that the stresses are primarily EV in origin. By analogy to our results for equilibrium rubber elasticity, it might be thought that in spite of the primary EV role in stress production, the use of the entropic spring concept, purely as a computational device, might again lead to a good quantitative estimate of the stresses. In contrast to the equilibrium regime, however, we find that the use of the entropic spring concept greatly underestimates the observed stresses, particularly in the early stages of the relaxation process. These results are in agreement with those obtained recently by Fixman,[5] who used a different model and method of simulation.

Our previous tests[4] of the range of validity in relaxation processes of the entropic spring concept as a computational device were for models corresponding to cross-linked networks. The purpose of the present study is to perform simulations of stress relaxation in model polymer melts in order to determine at which stage, if any, the entropic spring concept may be employed, as a computational device, to provide an accurate estimate of the EV generated stress.

The outline of this paper is as follows: The model polymer melt system employed is described in section 2, and the method used to simulate stress relaxation, which is an extension of that described in ref 4, is presented in section 3. The results, insofar as they relate to stress histories, are then presented in section 4. We then turn, in section 5, to the development of segment orientation in the melt during a time-dependent deformation process and consider this question together with the corresponding stress history as it relates to the stress-optical coefficient. Conclusions are presented in section 6.

2. Model System

The model system of the dense polymer melt used in this work is the same as that used in our previous work,[4] that is, a system of freely jointed chains with EV interaction represented by the repulsive part of the Lennard-Jones potential. The covalent bonds are linear stiff springs with zero force length a. The parameter σ of the Lennard-Jones potential corresponds closely to the effective hard-sphere diameter of the monomers; in the present simulation $\sigma = a$. Each chain has N bonds and $N+1$ atoms. Periodic boundary conditions are employed; the basic cell contains ν chains. The reduced density of the system is defined as $\rho = n\sigma^3/v$ where n/v is the monomer number density and $n = \nu(N+1)$. The reference time unit used in our simulation is $t_0 = \sqrt{m/\kappa}$ where m is the monomer mass and κ is the force constant of covalent potential. A reference temperature T_0 and a reference volume v_0 are defined as in ref 4. For the parameter values used there, we may also write $t_0 = 0.071(m\sigma^2/kT_0)^{1/2}$. For m and σ corresponding to the CH_2 monomer and $T_0 = 300$ K, $t_0 = 7.2 \times 10^{-14}$ s.

0024-9297/92/2225-3462$03.00/0

3. Method

The general method we employ for the simulation is similar in many respects to that of our previous viscoelastic study.[4] As described there, a constant-temperature molecular dynamics simulation is used. A time-dependent deformation history is imposed on the system by subjecting the periodic cell, initially cubic, to this deformation. In the terminology of ref 6, we are employing a boundary-driven algorithm. We have verified that the deformation information is transmitted from the boundaries to the cell interior with negligible inertia effects by running check simulations on smaller systems; we find that the resulting stress histories are substantially size-independent.

In our previous simulations, the basic procedure involved was based on the application of a time-dependent pure shear deformation that corresponded to constant simple shear rate $\dot{\gamma}$. This approach worked satisfactorily and provided values for the shear relaxation modulus $G(t)$ that decayed through 3 orders of magnitude. However, application of a constant shear strain rate $\dot{\gamma}$ limits the length of the simulation, since eventually the basic cell becomes too distorted. The simulation procedure employed in this work differs in the following ways: (a) The deformation imposed corresponds to elongation in the x_1 direction at constant volume rather than to shear. (b) The deformation corresponds to a short period at constant strain rate, followed by a long period at zero strain rate. This procedure permits the simulation of long relaxation periods without excessive distortion of the basic cell. In particular, we are able to extend the simulations reported here to periods that are 20 times longer than those in ref 4. The other advantage of the use of free relaxation is that it eliminates any concern regarding boundary-driven imposition of high strain rate. Rather, the relaxation result can be interpreted as corresponding to zero strain rate behavior.

During the simulation, the imposed elongation strain rate $\dot{\epsilon}_1$ is

$$\dot{\epsilon} = \begin{cases} \dot{\epsilon}_1^0, & 0 < t < t_1 \\ 0, & t > t_1 \end{cases} \tag{2}$$

where t_1 is the time when the relaxation starts.

Since the mean pressure in the system is of no interest, we focus on the difference stress $t_{11} - t_{22} = \sigma_1$, where $\sigma_1(t)$ is computed from the simulation results by the virial stress formula[4]

$$vt_{ij} = -n_t kT\delta_{ij} + \sum_{\alpha \in c} \langle r_\alpha^{-1} u_c'(r_\alpha)\, r_{\alpha i} r_{\alpha j} \rangle + \sum_{\alpha \in nc} \langle r_\alpha^{-1} u_{nc}'(r_\alpha)\, r_{\alpha i} r_{\alpha j} \rangle \tag{3}$$

where t_{ij} are the components of the stress tensor (force per unit present area) referred to the fixed rectangular Cartesian system x_i (i = 1–3), n_t is the number of atoms free to undergo thermal motion, δ_{ij} is the Kronecker delta, $\mathbf{r}_\alpha$ is the vector displacement between the α pair with components $r_{\alpha i}$, $r_\alpha = |\mathbf{r}_\alpha|$, $u_\alpha(r_\alpha)$ is the pair potential acting between the α pair, $u_\alpha' = du_\alpha/dr_\alpha$, brackets denote long-time averages, and the notations $\alpha \in$ c or $\alpha \in$ nc indicate that the sums range over all pairs of covalently or non-covalently interacting atoms, respectively. This formula permits a clear decomposition of σ_1 into the portion due to covalent interactions and that due to EV interactions. Because of the fluctuations inherent in the small size of the system, the initial stress $t_{ij}(0)$ is nonzero in an arbitrarily selected initial configuration. For this reason it is necessary to repeat the simulations n' times, using n' independent initial configurations and then averaging the results to obtain the desired physical quantities. Typically $n' = 120$ for the initial period of simulation and is gradually reduced (by stopping and discarding histories) to $n' = 15$ for the final portion of the relaxation period. This reduction in the number of trajectories or histories is possible because the rate of change of stress decreases in the latter periods and time averages may be taken over longer intervals.

The analysis of the simulation results proceeds as follows: Under the assumptions of the theory of linear viscoelasticity, it follows from the uniaxial, constant volume character of the imposed deformation that[7]

$$\sigma_1(t) = 3\int_0^t G(t-t')\, \dot{\epsilon}_1(t')\, dt' \tag{4}$$

where $G(t)$ is the shear relaxation modulus. It is assumed that the modulus $G(t)$ can be written as a Prony series

$$G(t) = \sum_{i=1}^{N'} g_i e^{-t/\lambda_i} \tag{5}$$

It then follows from eq 4 and the strain history, eq 2, that

$$\sigma_1(t) = \begin{cases} 3\dot{\epsilon}_1^0 \sum_{i=1}^{N'} g_i\lambda_i(1 - e^{-t/\lambda_i}), & 0 < t < t_1 \\ 3\dot{\epsilon}_1^0 \sum_{i=1}^{N'} g_i\lambda_i(e^{-(t-t_1)/\lambda_i} - e^{-t/\lambda_i}), & t > t_1 \end{cases} \tag{6}$$

We then employ a nonlinear least-squares fitting procedure to determine a single set of parameters g_i and λ_i in eq 6 that best fits the stress history $\sigma_1(t)$ determined from the computer simulation over both the loading and relaxation periods. The main algorithm is a Monte Carlo random search to find the least-squares deviation. The advantage of this method is that one can start from a set of parameters that are not very close to their optimal values, and the probability of being trapped in a local minimum is relatively small. We also used the Levenberg–Marquardt method[8] to speed up the calculation when the parameters become close to their optimal values. The number N' of modes used generally corresponded to roughly 1 mode per decade of time. Before beginning the fitting process over the complete loading and relaxation period, a preliminary fit, using one mode, was made to the time period $0 \le t < 5t_0$. This fit was used to determine $G_g = G(0)$; this value of G_g was then used as a constraint on the parameter selection for the full-history fit.

4. Stress

A typical simulated stress history $\sigma_1(t)$ is shown in Figure 1. Shown also are the separate covalent and EV contributions to this stress. As in our previous work, as well as in the work of Fixman,[5] it is clear that it is the EV interactions that are responsible for the stress during both the loading and the relaxation part of its history. In fact, the covalent contribution to $\sigma_1(t)$ is negative throughout all of its history except for a very short period at the beginning. This negative contribution is a consequence of the fact, observed as well in previous simulations,[9] that the covalent bond force is negative (compressive) at this value of reduced density.

We also compute the time-dependent stress tensor t_{ij} in the system by means of the expression[3]

$$t_{ij}(t) = \frac{1}{v} \sum_\beta \langle f_i(\beta)\, R_j(\beta) \rangle \tag{7}$$

where v is the system volume, $R_j(\beta)$ are the components

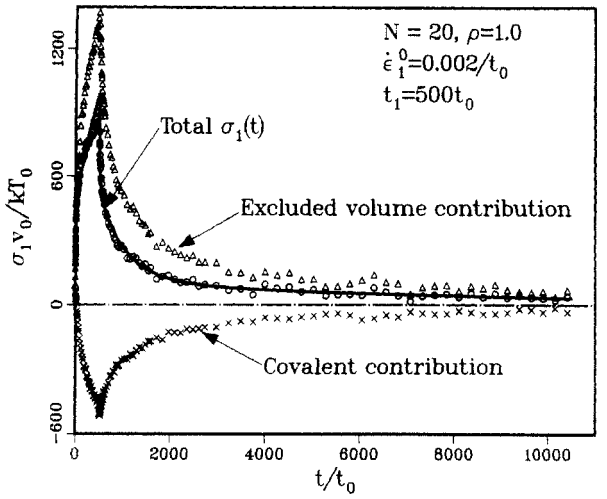

Figure 1. Stress history $\sigma_1(t)$ corresponding to the elongational strain history of eq 2. The solid curve is fitted through computed points of $\sigma_1(t)$ obtained by the fit to eq 6. Also shown are excluded-volume and covalent contributions to $\sigma_1(t)$. For parameters corresponding to polyethylene and with T_0 = 300 K, kT_0/v_0 = 0.053 MPa and $t_0 = 7.2 \times 10^{-14}$ s.

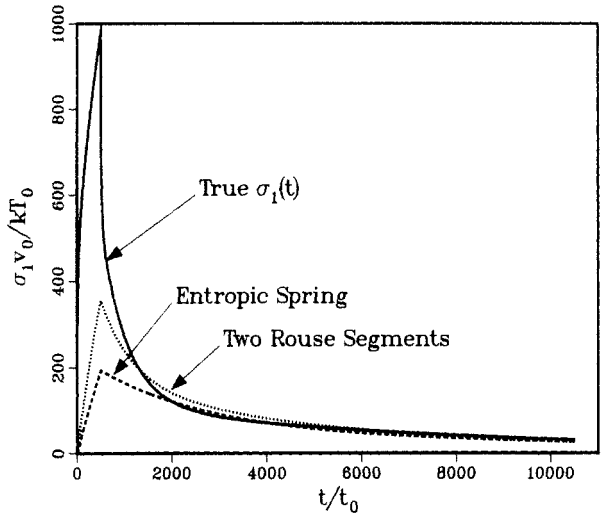

Figure 2. Comparison of stress history $\sigma_1(t)$ as computed on the basis of eq 7 by (a) regarding each whole chain as an entropic spring and (b) dividing each chain into two Rouse segments. The curve labeled "true $\sigma_1(t)$" is computed from simulation data by the virial stress formula, eq 3. Simulation conditions are the same as those in Figure 1.

of the chain vector of chain β at time t, $f_i(\beta)$ are the corresponding components of the chain force computed on the assumption of finite ideal entropic chain behavior,[2] and the sum is over all of the chains.[10] The carats represent an ensemble average over the histories corresponding to the ensemble of independent initial conditions for which simulations are performed. The results are shown in Figure 2. It is seen that the entropic spring stress greatly underestimates the true stress at the early stages, but the two appear to approach each other at later times.

The relaxation modulus $G(t)$ obtained from the stress history $\sigma_1(t)$ by the fitting procedure described above is shown in Figure 3. Also shown there is the value for $G(t)$ obtained by fitting the stress history based on the entropic spring calculation. It is seen that the true value of $G(t)$ decays, in the simulation period, over 3 orders of magnitude from a value G_g appropriate for the glassy state to a value on the order of G_r appropriate for the rubbery state. The entropic spring $G(t)$, on the other hand, begins from the outset at a value close to G_r; the true and entropic spring moduli approach each other only when the

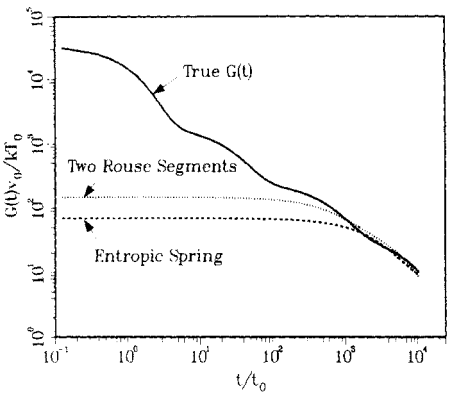

Figure 3. Relaxation modulus $G(t)$ corresponding to the three stress histories shown in Figure 2.

true $G(t)$ reaches the rubbery range.

Rouse Segments. In most theoretical treatments of polymer melt dynamics,[11] the chains are regarded as divided into subchains, called Rouse segments, and eq 7 is applied to the system of Rouse segments. In the theoretical treatments, these subchains are taken as sufficiently long so that they can be treated as Gaussian. In our simulations the chains themselves are too short to be treated as Gaussian, and, of course, the same is the case for any subdivisions. Nevertheless, it is of interest to consider each chain of the system as consisting of two subchains, that we term Rouse segments, and to apply eq 7 summed over all subchains with the chain force again computed on the assumption of finite ideal entropic chain[2] behavior.

The resulting stress history is shown in Figure 2 and the corresponding $G(t)$ in Figure 3. It is seen that whether the chains are regarded as consisting of one entropic spring or two Rouse segments makes little difference in the later, rubbery regime; there both methods are in substantial agreement with each other and with the true stress history. The situation is different in the earlier part of the stress history. There use of two Rouse segments in place of one entropic spring approximately doubles the stress level and the relaxation modulus $G(t)$. However, these values remain far below the actual histories as determined from the virial theorem. Since with two Rouse segments per model chain of N = 20 each segment has only 10 bonds, the increased values in the earlier stages noted in this case reflect an effective upper bound to the increase possible by chain subdivision.

Simulated Plateau. As seen from Figure 3, the simulated true $G(t)$ does not exhibit an extended plateau regime. This is not surprising since the model chains have only N = 20 bonds. In order to explore the effect that a plateau might have, we simulate what we have termed[2] an oriented melt. This is a melt in which all atoms are free to undergo thermal motion except that the end-to-end vectors $\mathbf{R}(\beta)$ of each chain β are maintained constant. Here, the oriented melt is obtained from a free melt subjected to a constant volume elongation, with all chain vectors fixed when the extension ratio λ = 2. In this deformed state the system is permitted to come to equilibrium, leading to a constant value for σ_1. This situation we regard here as modeling a plateau regime in which the entanglements are stable for a long period. Then, at a time we designate as t = 0, we model the simultaneous release of all entanglements by removing all constraints on the chain vectors, and $\sigma_1(t)$ therefore begins to relax toward zero. For both the plateau period and the relaxation we compute both the true stress history $\sigma_1(t)$ by use of the virial formula and the entropic spring stress history, based on one en-

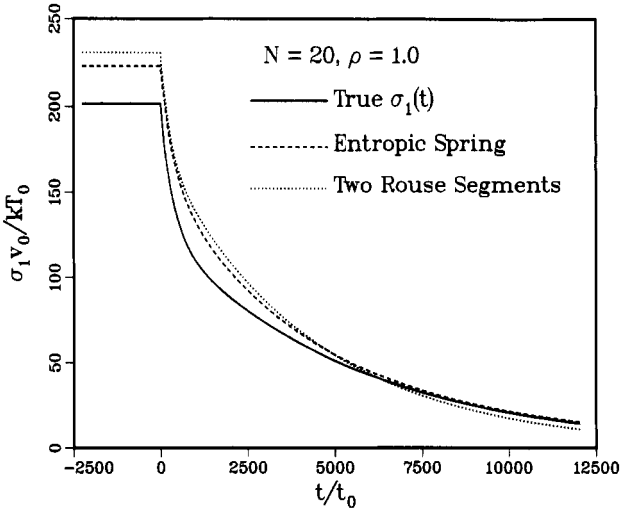

Figure 4. Simulated terminal relaxation from the plateau regime, computed on the basis of the three methods listed in Figure 2. The method of producing a simulated plateau is described in the text.

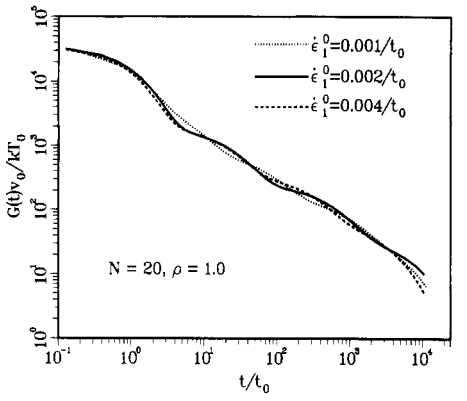

Figure 5. Comparison of relaxation modulus $G(t)$ obtained from simulations with the deformation history of eq 2 for three different values of $\dot{\epsilon}_1^0$. The unloading time t_1 is chosen so that the product $\dot{\epsilon}_1^0 t_1 = 1$ in all three cases.

tropic spring or on two Rouse segments, by use of eq 7. All three histories are fitted by a sum of exponentials by a procedure analogous to that previously described. The results are shown in Figure 4 where it is seen that the three methods of computation are in reasonably good agreement.

Effect of Strain Rate. Simulations were performed at three different values of $\dot{\epsilon}_1^0$ with values of t_1 chosen so that the product $\dot{\epsilon}_1^0 t_1$ remained constant. The resulting values of $G(t)$ are shown in Figure 5, where it is seen that, in keeping with the theory of linear viscoelasticity, the three results are in good agreement.

Shear Deformation. In ref 4 the simulation procedure determined $G(t)$ on the basis of a time-dependent pure shear deformation that corresponded to constant simple shear rate $\dot{\gamma}_0$ for $0 < t < t_1$. Here it is extended to include an unloading process, $\dot{\gamma} = 0$ for $t > t_1$. For the same system parameters, we compare, in Figure 6, the values of $G(t)$ determined for simple shear with those obtained on the basis of constant-volume elongation.

The good agreement obtained for these two independent simulations, as well as the agreement between the three simulations at different strain rates (Figure 5), serves to demonstrate not only the degree of applicability of the theory of the linear viscoelasticity to our model but also the degree of reproducibility and accuracy of the overall simulation and fitting procedure employed.

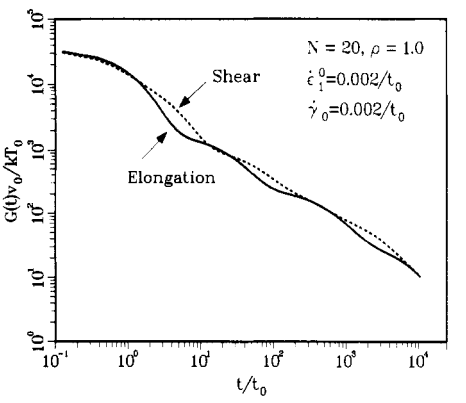

Figure 6. Comparison of relaxation modulus $G(t)$ obtained from simulations in which (a) the deformation is an elongation with a history given by eq 2 and (b) the deformation is shear as described in the text. The unloading time $t_1 = 500t_0$ in both cases.

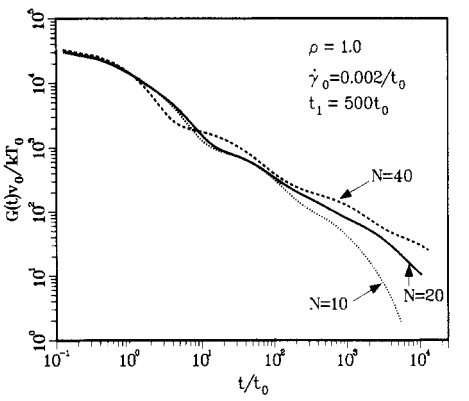

Figure 7. Effect of chain length on the relaxation modulus $G(t)$. The deformation is shear with history analogous to eq 2.

Effect of Chain Length. Simulations were performed, using shear deformation, for three systems with chains with $N = 10$, 20, and 40 bonds. The results for $G(t)$ are shown in Figure 7. In the earlier relaxation period the results are, except for statistical scatter, N independent, but the latter relaxation period shows a clear N dependence. Both effects are in accord with what is observed experimentally.[12]

5. Segment Orientation

The segment orientation $P_2(t)$ is computed at each time t during the simulation where

$$P_2(t) = \frac{1}{2}(3\langle \cos^2 \theta \rangle - 1) \tag{8}$$

and where $\theta(t)$ is the angle at time t between the segment and the stretch direction, with the average carried out over all of the segments of the system and over the ensemble of initial conditions. The variation of $P_2(t)$ is shown in Figure 8 for the simulation whose stress history $\sigma_1(t)$ is shown in Figure 1. Comparison of these two figures reveals that the nature of the variations of $\sigma_1(t)$ and $P_2(t)$ are quite similar. This suggests the introduction of an orientation relaxation modulus $R(t)$ such that, in analogy to eq 4

$$P_2(t) = \int_0^t R(t-t')\, \dot{\epsilon}_1(t')\, dt' \tag{9}$$

and the representation of $R(t)$ by a Prony series

$$R(t) = \sum_{i=1}^{N'} h_i e^{-t/\mu_i} \tag{10}$$

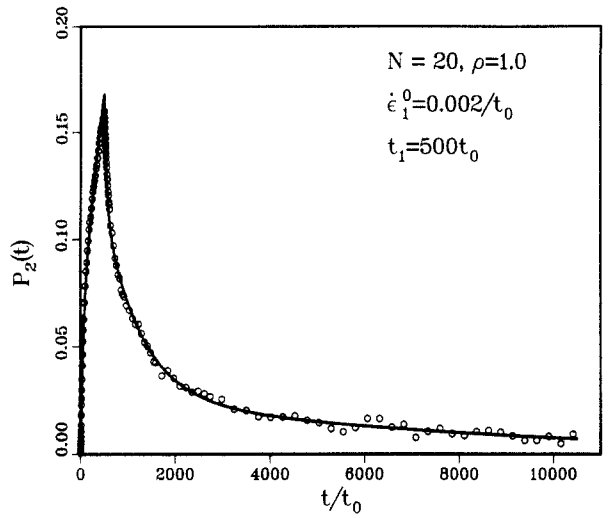

Figure 8. Time history of segment orientation $P_2(t)$, eq 8, for the simulation described in Figure 1. Solid curve is fitted through simulation points by use of a Prony series as described in the text.

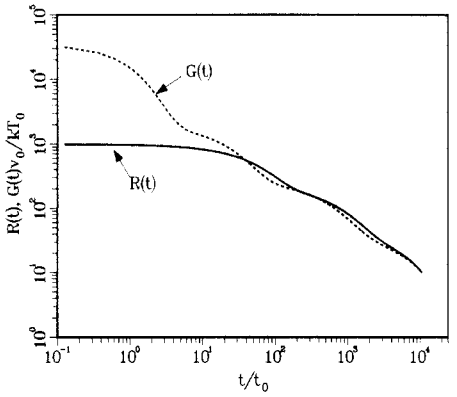

Figure 9. Comparison of orientation relaxation modulus $R(t)$ for the orientation history of Figure 8 with corresponding stress relaxation modulus $G(t)$. Values of $R(t)$ (dimensionless) are scaled to produce agreement with $G(t)$ v_0/kT_0 at $t/t_0 = 10^4$.

Table I
Modal Parameters for Stress and Orientational Moduli[a]

$N = 20$	$\nu = 48$	$\rho = 1.0$	$T = 300$ K	$\dot{\epsilon}_1^0 = 2.78 \times 10^{10}$ s^{-1}
Stress Relaxation Modulus				
$\lambda_1 = 0.077$	$\lambda_2 = 1.69$	$\lambda_3 = 34.2$	$\lambda_4 = 61.5$	$\lambda_5 = 593$
$g_1 = 1780$	$g_2 = 87.8$	$g_3 = 8.95$	$g_4 = 2.71$	$g_5 = 1.92$
Orientation Relaxation Modulus				
$\mu_1 = 0.53$	$\mu_2 = 3.92$	$\mu_3 = 55.4$	$\mu_4 = 544$	
$h_1 = 0.037$	$h_2 = 0.498$	$h_3 = 0.118$	$h_4 = 0.027$	

[a] Units employed are as follows: λ_i, μ_i, 10^{-12} s; g_i, MPa.

so that the predicted $P_2(t)$ for the given strain history is then analogous to eq 6. The Prony series parameters h_i and μ_i that best fit the observed $P_2(t)$ are then obtained by the same procedure as followed for the observed $\sigma_1(t)$. The resulting fit to the observed $P_2(t)$ is shown in Figure 8. The corresponding $R(t)$ is compared with $G(t)$ in Figure 9. The values of the parameters for $G(t)$ and $R(t)$ for this case are listed in Table I. Note that the shortest time constant μ_1 in the Prony series for $R(t)$ is only about 7 times that of λ_1 for $G(t)$. However, the weight h_1 of this mode is negligible. The shortest significant time constant, μ_2, is $\sim 50\lambda_1$.

With the availability of fitted curves to both $P_2(t)$ and $\sigma_1(t)$, it is of interest to compute their ratio, $r(t) = P_2(t)/\sigma_1(t)$, a quantity that plays a key role in discussions of the stress-optical coefficient. The result is shown in Figure 10. The most notable feature is the transition from

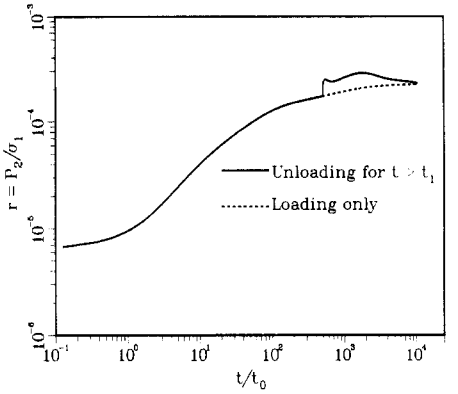

Figure 10. Ratio $r(t) = P_2(t)/\sigma_1(t)$ where $P_2(t)$ is shown in Figure 8 and $\sigma_1(t)$ is shown in Figure 1 (solid line). The dashed line is for deformation history $\dot{\epsilon}_1(t) = \dot{\epsilon}_1^0$ for $t > 0$ (no unloading). Units of r are v_0/kT_0 (see caption to Figure 1). The jump in the solid curve is discussed in the text; see eq 11.

relatively low values of r in the glassy regime to a much higher range in the rubbery regime. This result would appear to be related to the experimental fact that the stress-optical coefficient for solids is much smaller in magnitude than that for the corresponding rubber or melt.[13]

Another feature observed in Figure 10 in the behavior of $r(t)$ is the jump Δr at time t_1 when, eq 6, unloading begins. This jump is a direct consequence of the fact, as seen in Table I and in Figure 9, that the model parameters for $G(t)$ contain a very fast mode, g_1, λ_1, that is absent from those for $R(t)$. By consideration of eq 6 and the corresponding equation for $P_2(t)$, it may be shown that

$$\Delta r \simeq r(t_1+\lambda_1) - r(t_1) \simeq \frac{3\dot{\epsilon}_1^0 g_1 \lambda_1 (1-e^{-1}) r(t_1)}{\sigma_1(t_1) - 3\dot{\epsilon}_1^0 g_1 \lambda_1 (1-e^{-1})} \quad (11)$$

The numerical value for Δr predicted by eq 11 is in very good agreement with that shown in Figure 10. With the analytical expressions available for $G(t)$ and $R(t)$, it is straightforward to compute the ratio $r(t)$ for other deformation histories. The result for $\dot{\epsilon}_1(t) = \dot{\epsilon}_1^0$ for $t > 0$ (i.e., with no unloading) is also shown in Figure 10.

A recent interesting paper by Wimberger-Friedl and De Bruin[14] dealing with the time-dependent stress-optical behavior of polycarbonate came to our attention after the completion of the present work. They treat their experimental data with a time-dependent stress-optical law in close analogy to our eq 9. Their experimental results, shown in their Figure 6, when subjected to temperature–time shifting, bear close similarity to our Figure 10. Whereas our ratio of rubbery to glassy values is approximately 35, their corresponding ratio is approximately 55.

6. Conclusions

The principal conclusions of this work can be summarized briefly as follows:

(1) The relaxation stresses in a deformed polymer melt arise from the screened EV interactions, not from the forces in the covalent bonds of the chains.

(2) Prior to the rubbery regime in the relaxation process, use of the entropic spring concept as a computational device greatly underestimates the true stress history and the relaxation modulus $G(t)$.

(3) The entropic spring concept and associated ideal chain forces may be used to provide a good estimate of the relaxing stress starting with the plateau regime and continuing through the terminal regime.

Our observation that the entropic spring concept and the associated Rouse chain model are inapplicable, in particular, in the glassy regime is in accord with views that have long been expressed by others. We may refer, for example, to the recent paper by Ferry[15] giving some historical background. This observation may be understood and supported from several viewpoints. (a) The concept of the configurational entropy of a long-chain molecule with a fixed end-to-end distance is meaningful only when referred to a time period in which the chain has been able to sample the various conformations available to it. The glassy regime properly corresponds to a time period (whose length is determined by the atomic mobility of the system) in which its atoms execute small-amplitude vibrations[16] in the vicinity of fixed positions in space. In this time period chains do not change their conformations. (b) As a consequence of the localized vibrations of the atoms in the glassy regime, the elastic behavior of the system can be described with reasonable accuracy by the quasi-harmonic approximation.[17] A consequence of this approximation is that the elastic constants, in particular G_g, have only a weak temperature dependence, generally a small softening with a temperature increase at constant pressure. This is in accord with experimental observations.[18] The use of models based on the entropic spring concept, on the other hand, predicts that G_g is proportional to absolute temperature T. (c) While our simulations give numerical values of G_g that are in the range of those observed experimentally, use of the entropic spring concept in terms of Rouse models with reasonable segment size leads to values of G_g that are about 2 orders of magnitude too small.[13] (d) Our simulations, in agreement with experiment, lead to values of G_g that vary little (see Figure 7) with chain length. (e) The ratio r of segment orientation to stress (Figure 10) is much smaller in the glassy regime than in the rubbery regime. This may be traced to the existence of a very fast mode in the stress relaxation modulus $G(t)$ that is absent in the orientation modulus $R(t)$. (See Table I and Figure 9.) This very fast mode has its numerical counterpart[4] in the simple fluid formed from the melt by eliminating all covalent bonds; i.e., it corresponds to a mode of deformation, atomic ordering, that does not involve the covalent bonds to any significant extent.

The shortcomings of the entropic spring concept as a computational device are, as detailed above, most obvious in the glassy regime. Our simulations show, as noted, that this concept continues to be a poor basis for stress computation in polymer melts until the rubbery regime is reached. It appears that theories for the earlier regimes must include nonbonded (in particular, excluded-volume) interactions in a central fashion.

We have arrived at these conclusions through simulations of polymer melts of short freely-jointed model chains. A natural question that arises is whether these conclusions are due to the idealized character of the simulated system and have little or no relevance to real systems. We believe this is not the case for the following reasons: (1) We find that, in the glassy regime and in early time relaxation from it, the stresses both in the model melt and in the corresponding simple fluid obtained by eliminating all covalent bonds are quantitatively very close to each other.[4] This demonstrates clearly the EV origin of the stresses and suggests that the nature of the bond structure and the length of the chain, completely absent in the simple fluid, plays a relatively little role in this regime. (2) Our conclusion that the stress is due to nonbonded EV interactions and not to the backbone forces is in accord with the recent results of Fixman,[5] who used a very different chain model, one designed to represent long chains with some stiffness, and determined the stress relaxation modulus $G(t)$ on the basis of an equilibrium Green–Kubo simulation, whereas we employed nonequilibrium molecular dynamics. (3) Our simulations reveal two different mechanisms whereby the spherically symmetric two-body EV potential makes an anisotropic contribution to the stress. In the glassy regime this comes about through a transient atomic ordering[4] induced by the macroscopic strain. This mechanism is present as well in the simple fluid. In the rubbery regime the EV anisotropic contribution may be explained in terms of the screening of the EV interaction by the covalent structure which has been rendered anisotropic by the imposed deformation. It appears likely to us that these mechanisms will be operative, as well, when more realistic chain models are involved. Although we believe, therefore, that our basic conclusions in broad outline are not artifacts of the simple model employed, it is clearly important to investigate the extent to which they will be modified when more realistic models are employed. We hope to perform such studies in the future.

Acknowledgment. This work was supported by the Gas Research Institute (Contract No. 5091-260-2237) with the computations performed on the Cray Y-MP at the Pittsburgh Supercomputer Center.

References and Notes

(1) Guth, E.; Mark, H. *Monatsh. Chem.* **1934**, *65*, 93.
(2) Gao, J.; Weiner, J. H. *Macromolecules* **1991**, *24*, 1519.
(3) Gao, J.; Weiner, J. H. *Macromolecules* **1991**, *24*, 5179.
(4) Gao, J.; Weiner, J. H. *Macromolecules* **1992**, *25*, 1348.
(5) Fixman, M. *J. Chem. Phys.* **1991**, *95*, 1410.
(6) Evans, D. J.; Morriss, G. P. *Statistical Mechanics of Nonequilibrium Liquids*; Academic Press: London, 1991; pp 133–146.
(7) A preliminary brief account of some of this work has been given in an ACS Division of Polymer Chemistry preprint for presentation at the April 1992 annual meeting. There we employ the terminology $E(t)$ for what is here termed $3G(t)$.
(8) Press, W. H.; Flannery, B. P.; Teukolsky, S. A.; Vetterling, W. T. *Numerical Recipes*; Cambridge University Press: Cambridge, U.K., 1986; pp 523–528.
(9) See, for example, Figure 4 of: Gao, J.; Weiner, J. H. *Macromolecules* **1989**, *22*, 979.
(10) Note that we are using the convention, customary in solid mechanics, of positive tensile stress.
(11) See, for example: Doi, M.; Edwards, S. F. *The Theory of Polymer Dynamics*; Clarendon: Oxford, U.K., 1986.
(12) See, for example: Tobolsky, A. V. *Properties and Structures of Polymers*; John Wiley: New York, 1960; p 149.
(13) Inoue, T.; Okamoto, H.; Osaki, K. *Macromolecules* **1991**, *24*, 5670. Williams, M. L. *J. Polym. Sci.* **1962**, *62*, S7.
(14) Wimberger-Friedl, R.; De Bruin, J. D. *Rheol. Acta* **1991**, *30*, 419.
(15) Ferry, J. D. *Macromolecules* **1991**, *24*, 5237 (see the discussion at the lower right of 5239). See also ref 12, p 171.
(16) Zallen, R. *The Physics of Amorphous Solids*; John Wiley: New York, 1983; p 14.
(17) Weiner, J. H. *Statistical Mechanics of Elasticity*; John Wiley: New York, 1983.
(18) Ferry, J. D. *Viscoelastic Properties of Polymers*, 3rd ed.; John Wiley: New York, 1980; pp 304–305.